optica

Generation of second-harmonic beams with switchable curved trajectories

Sivan Trajtenberg-Mills,[1,*] Irit Juwiler,[2] and Ady Arie[1]

[1]School of Electrical Engineering, Faculty of Engineering, Tel-Aviv University, Tel-Aviv 69978, Israel
[2]Department of Electrical and Electronics Engineering, Sami Shamoon College of Engineering, Ashdod 77245, Israel
*Corresponding author: sivantra@mail.tau.ac.il

Received 21 June 2016; revised 28 November 2016; accepted 30 November 2016 (Doc. ID 268956); published 19 January 2017

Beams which follow curved trajectories are useful in a variety of applications, but up to now have been realized mainly in linear media. We demonstrate theoretically and experimentally the generation of second-harmonic (SH) beams which follow arbitrary convex caustic trajectories. These beams are created in a nonlinear photonic crystal with a second-order susceptibility having a tailored pattern; hence, the SH beam follows the desired trajectory after exiting the crystal. The same crystal can incorporate more than one trajectory, enabling the nonlinear creation of bottle beams as well as beams with switchable caustic trajectories that can be controlled by the phase-matching conditions.

OCIS codes: (190.2620) Harmonic generation and mixing; (140.3300) Laser beam shaping; (090.1760) Computer holography; (050.5298) Photonic crystals.

https://doi.org/10.1364/OPTICA.4.000153

Light beams which follow a curved trajectory along their propagation have been a subject of great interest over the past years, owing both to their counterintuitive propagation dynamics in free space as well as their promise for applications in optical manipulation [1], material processing [2], light-sheet microscopy [3], etc. The first to exhibit this property was the Airy beam [4], the solution of the paraxial Helmholtz equation which follows a parabolic trajectory in free space. This beam is the optical equivalent of the quantum-mechanical Airy wave packet [5] as the solution to the Schrödinger equation for a free particle. The Airy beam has been realized in many different media, including free space [4], nonlinear optics [6], plasmon waves [7], electron waves [8], and recently even in water waves [9,10]. Other analytical solutions of beams with parabolic and elliptic trajectories exist in the nonparaxial regime [11].

The acceleration of these waves is a manifestation of a constructive interference pattern which follows some convex curved trajectory. For example, the ideal Airy beam has infinite energy and an infinite amount of lobes, allowing for it to accelerate infinitely since the beam energy along the curve arrives from the side lobes [12]. In reality the beams are truncated, usually using an exponential or Gaussian window, in order to maintain finite energy and therefore undergo diffraction and abandon their curved trajectory after some distance. Having understood this, one can create beams which follow arbitrary curved trajectories over a limited propagation distance (beyond the simple parabolic trajectory of the Airy beam) by tailoring constructive interference of waves along the desired trajectory. Each point along the desired trajectory $c(x)$ in the propagation axis x must have a corresponding tangent line at $x = 0$ with slope θ, which builds it constructively so that $dc(x)/dx = \tan\theta$. This can be parameterized using $dc(x)/dx = [c(x) - y]/x$, with y being the transverse axis. The transverse phase $\varphi(y)$ of the beam at $x = 0$ can then be derived geometrically [13]:

$$\frac{d\varphi(y)}{dy} = k\sin\theta = \frac{kc'(x)}{\sqrt{1+[c'(x)]^2}}, \tag{1}$$

where k is the wave vector and $c'(x) = dc(x)/dx$. This concept has been used before to create arbitrary convex trajectories in linear media such as free-space optics [13,14], plasmon waves [15], and acoustic waves [16]. Here, we demonstrate the nonlinear generation of beams with arbitrary caustic trajectories in a quadratic nonlinear medium, in the process of second-harmonic (SH) generation. SH beam-shaping has been achieved before by modulation of the second-order nonlinear susceptibility $\chi^{(2)}$ of a crystal in a discrete [17] or continuous manner [18]. In order to achieve the desired caustic trajectory in the SH, we encode the transverse phase on $\chi^{(2)}$ using binary computer-generated holograms [19]:

$$\chi^{(2)}(y,x) = \chi^{(2)}\,\mathrm{sign}\left\{\cos\left[\frac{2\pi}{\Lambda(\Delta k)}x + \varphi(y)\right]\right\}, \tag{2}$$

where x is the propagation direction, y is the transverse axis, and $\varphi(y)$ is the transverse phase which is calculated using Eq. (1). $\Lambda(\Delta k) = 2\pi/\Delta k$ is the modulation period used to compensate for the phase mismatch $\Delta k(\lambda, T)$ for a certain temperature T and input wavelength λ:

$$\Delta k(\lambda, T) = \frac{4\pi}{\lambda}\left[n(\lambda, T) - n\left(\frac{\lambda}{2}, T\right)\right]. \tag{3}$$

Here, $n(\lambda, T)$ is the refractive index of the photonic crystal at the input wavelength λ and temperature T. This results in a binary continuous curved periodic modulation of $\chi^{(2)}$ with very high curvature, considerably higher than the typical required

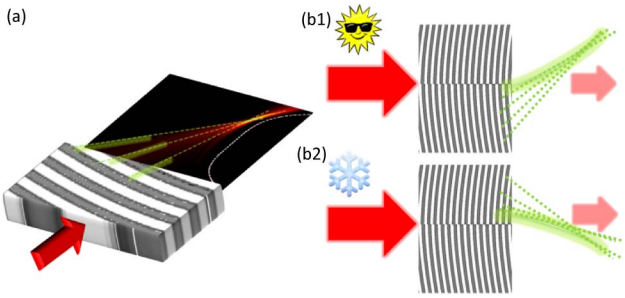

Fig. 1. (a) Schematic diagram of our experiment: the input laser beam (red) incident on the curved modulation of the crystal generates the SH beam (green) which follows a curved trajectory. (b) Switchable trajectories: the trajectory of the SH beam can be controlled by changing the temperature for a crystal with two different regions, each phase matching the fundamental beam at different temperatures.

curvatures in other applications [6,20]. The SH beam created in the crystal will acquire the transverse phase $\varphi(y)$ and therefore follow the planned trajectory upon exiting the crystal, as is illustrated in Fig. 1(a). The transverse phase can generally be calculated numerically. In the paraxial approximation, the phase of a polynomial trajectory $c(x) = ax^n$ can be calculated through [13]

$$\phi(y) = k_{2\omega} n^2 y^2 \frac{[a(1-n)/y]^{1/n}}{(2n-1)(1-n)}. \quad (4)$$

Here, $k_{2\omega}$ is the wave vector of the second-harmonic beam. In our work, the phase was calculated numerically but in most cases the difference between the numeric calculation and the analytic paraxial solution obtained from Eq. (4) was negligible.

Furthermore, we can design a crystal which has two regions with different phases $\varphi_1(y)$ and $\varphi_2(y)$, thereby creating different trajectories $c_1(x)$ and $c_2(x)$. By choosing two trajectories in opposite directions, we can create "bottle beams" [21], beams which consist of a dark central region that is fully surrounded by regions of high intensity. Optical bottle beams have been a subject of interest in recent years, mainly due to their attractive applications in optical tweezers for trapping and manipulation of small particles [22]. If the beams are launched at their vertex point, they need to be spatially separated in order to create a "hot spot" at their convergence. Since we control both the trajectory and the spatial separation, we can fully control the total shape of the bottle beam and the location of the "hot spot".

While this kind of shaping may also be achieved by different methods such as using a spatial light modulator before the crystal [23] or adding a mask after the crystal [24], unlike these, our method also enables the creation of a switchable device. The two different regions in the crystal can be planned to have two different carrier frequencies Λ_1 and Λ_2 which compensate for the phase mismatch $\Delta k_1(\lambda, T_1)$ and $\Delta k_2(\lambda, T_2)$ in two different temperatures (or alternatively at two different pump wavelengths), as is illustrated in Fig. 1(b). In this way, we obtain a temperature-controlled switch where, by changing the temperature of the crystal between the two different discrete phase-matching temperatures, the SH process will be efficient only in the region with the proper modulation period, so the generated SH beam will follow the corresponding caustic trajectory at the exit of the crystal. Since $\Delta k(\lambda, T)$ is a function of both the temperature and the input wavelength, the trajectory of the SH beam can also be controlled by changing the input pump wavelength. We note that another method for nonlinearly switching the trajectory was demonstrated previously for Airy beams [25], but it was based on selecting either a down-conversion process for one trajectory or an up-conversion process for the other trajectory. Here, a different switching process is used which relies on two phase-mismatch values for the same process.

In order to experimentally explore nonlinear generation of light beams with arbitrary caustic trajectories, we designed patterns for several different polynomial curves. We then fabricated these designs on stoichiometric lithium tantalate doped with 0.5% MgO (PP-Mg:SLT) crystals by electric field poling. The inverted domain structure was created by applying an electrical field upon a patterned electrode on the crystal surface. The maximum charge density was 60 $\mu C/cm^2$ and the maximum electric current density was 184.7 $\mu A/cm^2$. The poled structure was 0.7 mm long for all designs, and ranged from 1.4 to 0.98 mm in width. We used a 1064.5 nm Nd:YAG pulsed laser with 4.4 ns pulses at a 10 kHz repetition rate, working with a peak power of ~22 kW, as the fundamental beam. The beam was focused using a cylindrical lens to a size of 400 μm × 150 μm attained in the middle of the crystal. We used a CCD camera to measure the output result after filtering the fundamental beam. The crystal exit plane was imaged to the CCD camera using a lens, and the beam's propagation was measured in planes 0.25 mm apart over a total length of 12–40 mm.

First, we planned a non-monotonic curved polynomial trajectory of ax^4 ($a = 282251\ m^{-3}$) spanning from the negative side of the vertex to the positive side. The poling for this crystal was 7.88 μm, which phase-matches the laser wavelength at 100°C. The fabricated crystal exhibits the desired curved modulation, with some imperfections especially on the edges of the mask, as can be seen in Fig. 2(a). These places have the highest curvature and therefore require the highest fabrication resolution—a challenge for the poling process. This should cause the generated beam to follow the desired curve closely at low angles and deviate from it at higher angles. Simulation and experimental results can be seen in Fig. 2(b).

We also designed crystals which create "bottle beams." We chose different polynomial trajectories in different directions for each crystal: $\pm 0.437x^2$ and $\pm 10.93x^3$ (x given in meters), spatially separated by 160 μm. The location of the point of intersection between the two beams, the "hot spot", can be easily calculated to be at 13.5 mm and 19.4 mm from the crystal exit plane. Both simulated and experimental beams form the hot spot at approximately this location; results can be seen in Fig. 3. Here

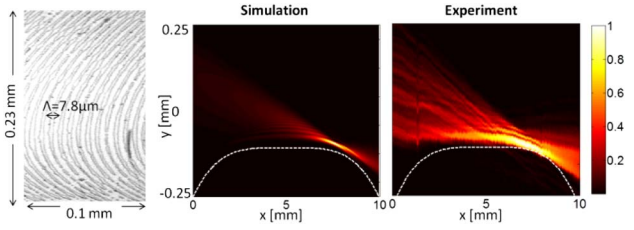

Fig. 2. Generation of a SH beam with a polynomial trajectory. (a) Microscopic photo of fabricated crystal. (b1) simulation and (b2) experimental results of SH beam propagation after the crystal, following the polynomial trajectory ax^4. The designed trajectory is shown as a white dotted line.

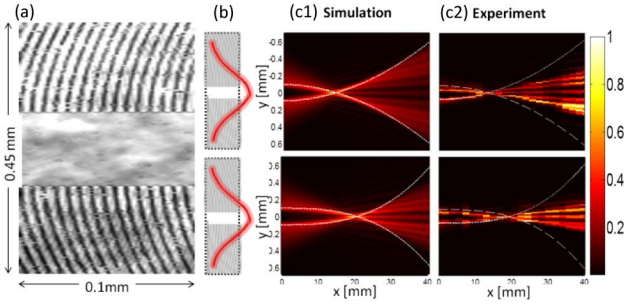

Fig. 3. SH generation of bottle beams. (a) Microscopic photo of fabricated crystal showing the two different curved periodic domains spatially separated. (b) Illustration of the crystal and pump beam, drawn to scale with the y axis. (c1) Simulation and (c2) experimental results for two different bottle beams, with parabolic (top) and quartic (bottom) trajectories. The dotted line shows the planned trajectory.

also, deviation from the designed mask at high angles hinders the regions of largest curvatures, but the general shape is conserved despite the defects in fabrication. The beams cease to follow the theoretical trajectory after the hot spot, owing to the finite width of the crystal in the transverse (y) direction and the finite size of the input pump beam. A wider crystal with a larger pump waist can generate a beam that will follow the theoretical trajectory over a larger distance [26].

Finally, we designed a crystal with a switchable caustic trajectory: two different poling periods of 7.77 and 7.98 μm were used, which phase-match our fundamental frequency laser at 50°C and 150°C, respectively. The different poled regions can be seen in Fig. 4(a), where a microscopic image of the middle of the crystal shows the two different periods. The designs used were polynomial trajectories of opposite signs, $c(x) = \pm bx^3 (b = 3.75\ \mathrm{m}^{-3})$. The change of trajectory can be also obtained by changing the input pump wavelength from 1064.5 to 1050.75 nm. Results can be seen in Fig. 4(b).

Conversion efficiencies of these beams are quite close to those of a simple periodically poled crystal of the same dimensions. A periodically poled crystal with the same dimensions as the bottle beam and switchable trajectory designs has a theoretical conversion efficiency of $1.84 \times 10^{-7}\ \mathrm{W}^{-1}$. Our simulated conversion efficiency ranged from 8.7×10^{-8} to $1.21 \times 10^{-7}\ \mathrm{W}^{-1}$, the lower

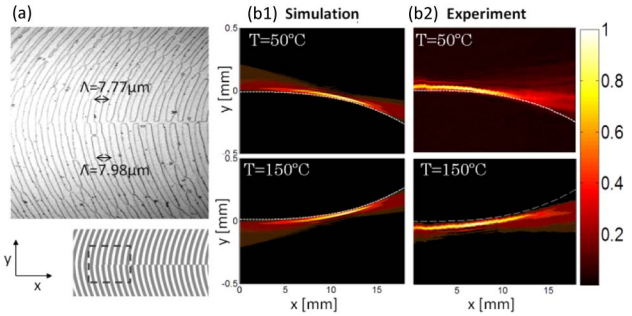

Fig. 4. Thermal switching of the caustic trajectory. (a) Microscopic photo of fabricated crystal (top), showing the two different curved periodic domains with different poling periods. Bottom shows the designed pattern, with the dotted square showing the location of the microscopic image in the crystal. (b1) Simulation and (b2) experimental results for 50°C (top) and 150°C (bottom). The dotted line shows the planned cubic trajectory.

efficiency being that of the switch since only half of the crystal area is efficient at each temperature, yielding an overall lower efficiency. Experimental SH peak power for the bottle beams ranged between 23 and 43 W, their corresponding efficiencies being 4.65×10^{-8} to $8.32 \times 10^{-8}\ \mathrm{W}^{-1}$, i.e., approximately 68% of the theoretical predicted efficiency. The SH peak power for the switched crystal was ~27 W with a corresponding efficiency of $\sim 4.7 \times 10^{-8}\ \mathrm{W}^{-1}$, i.e., approximately 54% of the theoretical predicted efficiency at both temperatures. The difference between the measured and simulated results is mainly due to defects in fabrication.

While the general method for caustic beam shaping can be applied to both paraxial and non-paraxial waves and can be used to create arbitrary convex trajectories [13,14], the nonlinear creation of these waves imposes limitations on the possible trajectories. One of these limitations arises from the limited resolution of the poling pattern. Through a geometric calculation [see Fig. 5(a)], the maximal bending angle θ of a ray can be easily calculated from the fabrication poling resolution

$$\theta = \cos^{-1}\left(\frac{\mathrm{RES} \cdot \Delta k}{\pi}\right), \tag{5}$$

where RES denotes the minimal feature size of the poled crystal and $\Delta k(\lambda, T)$ is the phase mismatch. While an SLT crystal can be poled in any angle [27], this limitation arises from the difficulty in creating very small domains. In our case, RES = 2 μm, thereby limiting the angle to ~60° for our range of wavelengths and temperatures.

A second limitation on the maximal bending angle is the length of propagation and beam width (and corresponding crystal width). Since the beams created at the input plane are tangent to the curve for a desired propagation distance Δx, the maximal bending angle for a beam with waist of W_0 (and a crystal wide enough to incorporate the entire beam) can be easily calculated geometrically [see Fig 5(b)] to be $\theta = \tan^{-1}(3 * W_0/\Delta x)$. This implies that, for longer distances Δx, the maximal angle is smaller. Also, larger pump waist helps create larger angles. In our experiment, this was the main restriction on the angle as we chose to work over long distances. The maximal angles measured in this work ranged between 0.2° and 7° (outside the crystal) due to the large propagation distances and relatively small pump waist.

Another limitation arises from the interaction length (crystal length). A short crystal generates caustic beams which closely follow the designed trajectory but exhibit low efficiency, while the beam generated in a longer crystal deviates largely from the designed trajectory but has higher efficiency. This tradeoff has been

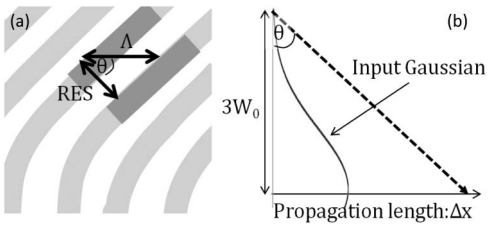

Fig. 5. Schematic illustration of the limitations described in the text: (a) corresponds to the limitation arising from the minimal resolution achievable by poling-RES and the constant poling period in x, Λ; (b) corresponds to the limitation arising from the input beam waist W_0 and the propagation length Δx.

analyzed before in the generation of plasmonic caustic beams, where the number of cycles creating the beam yields higher coupling efficiency [15] alongside deviation from the planned trajectory. The main reason for this effect is the accumulated phase gained by the created beam over the interaction length, which causes it to deviate from the original curve. Taking these considerations into account, we chose to work with relatively short crystals of 0.7 mm. Even in this short crystal length, both simulated and experimental beams do not follow the trajectory perfectly, mainly due to this phase accumulation.

Considering the nonlinear switchable trajectory crystal, a question arises as to what is the minimal temperature (or pump wavelength) difference that can be designed on the crystal for a noticeable change in the trajectory. This information is important for the ability to know how well this crystal can sense change in temperature or input pump wavelength. Assuming an undepleted, plane wave pump, the intensity of the SH beam created in a quasi-phase-matched crystal has the following dependence [28]:

$$I = \kappa \left[\frac{\sin((\Delta k - 2\pi/\Lambda)L/2)}{(\Delta k - 2\pi/\Lambda)L/2} \right]^2, \tag{6}$$

where κ is a coupling constant, Δk is the phase mismatch, Λ is the poling period, and L is the crystal length. For a distinguishable difference between the two trajectories we can require that, where one process that generates the first trajectory is most efficient, the second process should be at its first minimum. This leads to a simple separation condition:

$$\Delta k_1(\lambda_1, T_1) - \Delta k_2(\lambda_2, T_2) = \frac{2\pi}{L}. \tag{7}$$

By fixing the wavelength and solving this equation for a given crystal, the temperature sensitivity can be extracted. We can also calculate the wavelength sensitivity by fixing the temperature and choosing different wavelengths. Therefore we see that longer crystals can achieve better sensitivity, but as was shown before [15], the tradeoff is that the caustic beams may deviate from the planned trajectory. The exact temperature (wavelength) difference should be calculated according to the specific crystal's diffraction dependencies and changes accordingly. For instance, using a 0.7 mm long SLT crystal and a pump of 1064.5 nm, if the first peak is phase-matched at 100°C, the temperature sensitivity is ~40°C. Alternatively, for the same conditions, the wavelength sensitivity is ~4 nm. The sensitivity is greater in realms of strong dispersion.

In conclusion, we have generated second-harmonic beams having arbitrary polynomial trajectories by modulating the nonlinear coefficient so that it will quasi-phase-match the interaction and simultaneously impose the required transverse phase on the generated beam. To our knowledge, this is the first experimental generation of arbitrarily curved light beams in nonlinear interaction. The designs are not limited to the paraxial approximation and, with current operating parameters, the trajectory angles can reach 60° with respect to the optical axis. In addition, we integrated two different designs on a nonlinear single crystal; two spatially separated designs with opposite trajectories creating a bottle beam, as well as a nonlinear switch where the caustic trajectory is chosen according to the temperature of the crystal or the input pump wavelength. These nonlinear crystals provide a compact way of generating caustic beams in different wavelengths. Unlike other methods which exist for shaping the pump beam before or after a regular crystal, our method also enables the creation of a switchable device. We also evaluate the design limitations of this beam-generation process as well as the sensitivity of the nonlinear switch. Experimental results show good agreement with simulations, where the differences between them are caused by fabrication deviation from the planned mask.

Funding. Israel Science Foundation (ISF) (1310/13).

REFERENCES

1. J. Baumgartl, M. Mazilu, and K. Dholakia, Nat. Photonics **2**, 675 (2008).
2. A. Mathis, L. Froehly, L. Furfaro, M. Jacquot, J. M. Dudley, and F. Courvoisier, J. Eur. Opt. Soc. Rapid Publ. **8**, 13019 (2013).
3. T. Vettenburg, H. I. C. Dalgarno, J. Nylk, C. Coll-Lladó, D. E. K. Ferrier, T. Čižmár, F. J. Gunn-Moore, and K. Dholakia, Nat. Methods **11**, 541 (2014).
4. G. A. Siviloglou, J. Broky, A. Dogariu, and D. N. Christodoulides, Phys. Rev. Lett. **99**, 213901 (2007).
5. M. V. Berry and N. L. Balazs, Am. J. Phys. **47**, 264 (1979).
6. T. Ellenbogen, N. Voloch-Bloch, A. Ganany-Padowicz, and A. Arie, Nat. Photonics **3**, 395 (2009).
7. L. Li, T. Li, S. M. Wang, C. Zhang, and S. N. Zhu, Phys. Rev. Lett. **107**, 126804 (2011).
8. N. Voloch-Bloch, Y. Lereah, Y. Lilach, A. Gover, and A. Arie, Nature **494**, 331 (2013).
9. S. Fu, Y. Tsur, J. Zhou, L. Shemer, and A. Arie, Phys. Rev. Lett. **115**, 034501 (2015).
10. U. Bar-Ziv, A. Postan, and M. Segev, Phys. Rev. B **92**, 100301 (2015).
11. M. A. Bandres, I. Kaminer, M. Mills, B. M. Rodríguez-Lara, E. Greenfield, M. Segev, and D. N. Christodoulides, Opt. Photon. News **24**(6), 30 (2013).
12. Y. Kaganovsky and E. Heyman, Opt. Express **18**, 8440 (2010).
13. L. Froehly, F. Courvoisier, A. Mathis, M. Jacquot, L. Furfaro, R. Giust, P. A. Lacourt, and J. M. Dudley, Opt. Express **19**, 16455 (2011).
14. E. Greenfield, M. Segev, W. Walasik, and O. Raz, Phys. Rev. Lett. **106**, 213902 (2011).
15. I. Epstein and A. Arie, Phys. Rev. Lett. **112**, 023903 (2014).
16. S. Zhao, Y. Hu, J. Lu, X. Qiu, J. Cheng, and I. Burnett, Sci. Rep. **4**, 6628 (2014).
17. J. R. Kurz, A. M. Schober, D. S. Hum, A. J. Saltzman, and M. M. Fejer, in *Summaries of Papers Presented at the Lasers and Electro-Optics (CLEO '02)*, OSA Technical Digest (Optical Society of America, 2002), pp. 377–378.
18. S. Trajtenberg-Mills, I. Juwiler, and A. Arie, Laser Photon. Rev. **9**, L40 (2015).
19. W. H. Lee, Appl. Opt. **18**, 3661 (1979).
20. C. R. Phillips, B. W. Mayer, L. Gallmann, and U. Keller, Opt. Express **24**, 15940 (2016).
21. J. Arlt and M. J. Padgett, Opt. Lett. **25**, 191 (2000).
22. D. G. Grier, Nature **424**, 810 (2003).
23. A. Libster-Hershko, S. Trajtenberg-Mills, and A. Arie, Opt. Lett. **40**, 1944 (2015).
24. A. Shapira, A. Libster, Y. Lilach, and A. Arie, Opt. Commun. **300**, 244 (2013).
25. I. Dolev, T. Ellenbogen, and A. Arie, Opt. Lett. **35**, 1581 (2010).
26. F. Courvoisier, A. Mathis, L. Froehly, R. Giust, L. Furfaro, P. A. Lacourt, M. Jacquot, and J. M. Dudley, Opt. Lett. **37**, 1736 (2012).
27. D. Kasimov, A. Arie, E. Winebrand, G. Rosenman, A. Bruner, P. Shaier, and D. Eger, Opt. Express **14**, 9371 (2006).
28. R. W. Boyd, *Nonlinear Optics* (Academic, 2008).